# Discovery of a Jupiter/Saturn Analog with Gravitational Microlensing

B.S. Gaudi, D.P. Bennett, A. Udalski, A. Gould, G.W. Christie, D. Maoz, S. Dong, J. McCormick, M.K. Szymanski, P.J. Tristram, S. Nikolaev, B. Paczynski, M. Kubiak, G. Pietrzynski, I. Soszynski, O. Szewczyk, K. Ulaczyk, L. Wyrzykowski, D.L. DePoy, C. Han, S. Kaspi, C.-U. Lee, F. Mallia, T. Natusch, R.W. Pogge, B.-G. Park, F. Abe, I.A. Bond, C.S. Botzler, A. Fukui, J.B. Hearnshaw, Y. Itow, K. Kamiya, A.V. Korpela, P.M. Kilmartin, W. Lin, K. Masuda, Y. Matsubara, M. Motomura, Y. Muraki, S. Nakamura, T. Okumura, K. Ohnishi, N.J. Rattenbury, T. Sako, To. Saito, S. Sato, L. Skuljan, D.J. Sullivan, T. Sumi, W.L. Sweatman, P.C.M. Yock, M. Albrow, J.-P. Beaulieu, M.J. Burgdorf, K.H. Cook, C. Coutures, M. Dominik, S. Dieters, et al.

November 14, 2007

Science

**Disclaimer**

This document was prepared as an account of work sponsored by an agency of the United States government. Neither the United States government nor Lawrence Livermore National Security, LLC, nor any of their employees makes any warranty, expressed or implied, or assumes any legal liability or responsibility for the accuracy, completeness, or usefulness of any information, apparatus, product, or process disclosed, or represents that its use would not infringe privately owned rights. Reference herein to any specific commercial product, process, or service by trade name, trademark, manufacturer, or otherwise does not necessarily constitute or imply its endorsement, recommendation, or favoring by the United States government or Lawrence Livermore National Security, LLC. The views and opinions of authors expressed herein do not necessarily state or reflect those of the United States government or Lawrence Livermore National Security, LLC, and shall not be used for advertising or product endorsement purposes.

# Discovery of a Jupiter/Saturn Analog with Gravitational Microlensing

B.S. Gaudi[1,*], D.P. Bennett[2], A. Udalski[3], A. Gould[1],
G.W. Christie[4], D. Maoz[5], S. Dong[1], J. McCormick[6],
M.K. Szymański[3], P.J. Tristram[7], S. Nikolaev[8], B. Paczyński[9,†],
M. Kubiak[3], G. Pietrzyński[3,10], I. Soszyński[3], O. Szewczyk[3],
K. Ulaczyk[3], Ł. Wyrzykowski[3,11] (The OGLE Collaboration)
D.L. DePoy[1], C. Han[12], S. Kaspi[5], C.-U. Lee[13], F. Mallia[14],
T. Natusch[4], R.W. Pogge[1], B.-G. Park[13], (The μFUN Collaboration)
F. Abe[15], I.A. Bond[16], C.S. Botzler[17], A. Fukui[15], J.B. Hearnshaw[18],
Y. Itow[15], K. Kamiya[15], A.V. Korpela[19], P.M. Kilmartin[7], W. Lin[16],
K. Masuda[15], Y. Matsubara[15], M. Motomura[15], Y. Muraki[15], S. Nakamura[15],
T. Okumura[15], K. Ohnishi[21], N.J. Rattenbury[22], T. Sako[15], To. Saito[23],
S. Sato[24], L. Skuljan[16], D.J. Sullivan[19], T. Sumi[15], W.L. Sweatman[16],
P.C.M. Yock[17], (The MOA Collaboration)
M. Albrow[18], A. Allan[25], J.-P. Beaulieu[26], M.J. Burgdorf[27], K.H. Cook[8], C. Coutures[26],
M. Dominik[28], S. Dieters[29], P. Fouque[30], J. Greenhill[29], K. Horne[28],
I. Steele[27], Y. Tsapras[27],
(From the PLANET and RoboNet Collaborations)
B. Chaboyer[31], A. Crocker[32], S. Frank[1], B. Macintosh[8]

October 30, 2007

[1]Department of Astronomy, Ohio State University, 140 West 18th Avenue, Columbus, OH 43210, USA

*To whom correspondence should be addressed; E-mail: gaudi@astronomy.ohio-state.edu

[2]Department of Physics, 225 Nieuwland Science Hall, Notre Dame University, Notre Dame, IN 46556, USA

[3]Warsaw University Observatory, Al. Ujazdowskie 4, 00-478 Warszawa, Poland

[4]Auckland Observatory, P.O. Box 24-180, Auckland, New Zealand

[5]School of Physics and Astronomy, Raymond and Beverley Sackler Faculty of Exact Sciences,

Tel-Aviv University, Tel Aviv 69978, Israel

[6]Farm Cove Observatory, 2/24 Rapallo Place, Pakuranga, Auckland 1706, New Zealand

[7]Mt. John Observatory, P.O. Box 56, Lake Tekapo 8770, New Zealand

[8]IGPP, Lawrence Livermore National Laboratory, 7000 East Ave., Livermore, CA 94550, USA

[9]Princeton University Observatory, Princeton, NJ 08544, USA

[†]Deceased

[10]Universidad de Concepción, Departamento de Fisica, Casilla 160–C, Concepción, Chile

[11]Institute of Astronomy, University of Cambridge, Madingley Road, Cambridge CB3 0HA, UK

[12]Program of Brain Korea, Department of Physics, Chungbuk National University, 410 Seongbong-Rho, Hungduk-Gu, Chongju 371-763, Korea

[13]Korea Astronomy and Space Science Institute, 61-1 Hwaam-Dong, Yuseong-Gu, Daejeon 305-348, Korea

[14]Campo Catino Astronomical Observatory, P.O. Box Guarcino, Frosinone 03016, Italy

[15]Solar-Terrestrial Environment Laboratory, Nagoya University, Nagoya, 464-8601, Japan

[16]Institute for Information and Mathematical Sciences, Massey University, Private Bag 102-904, Auckland 1330, New Zealand

[17]Department of Physics, University of Auckland, Private Bag 92-019, Auckland 1001, New Zealand

[18]University of Canterbury, Department of Physics and Astronomy, Private Bag 4800, Christchurch 8020, New Zealand

[19]School of Chemical and Physical Sciences, Victoria University, Wellington, New Zealand

[20]Department of Physics, Konan University, Nishiokamoto 8-9-1, Kobe 658-8501, Japan [21]Nagano National College of Technology, Nagano 381-8550, Japan

[22]Jodrell Bank Observatory, The University of Manchester, Macclesfield, Cheshire SK11 9DL, UK

[23]Tokyo Metropolitan College of Aeronautics, Tokyo 116-8523, Japan

[24]Department of Physics and Astrophysics, Faculty of Science, Nagoya University, Nagoya 464-860, Japan

[25]School of Physics, University of Exeter, Stocker Road, Exeter, EX4 4QL, UK

[26]Institut d'Astrophysique de Paris, CNRS, Universit Pierre et Marie Curie UMR7095, 98bis Boulevard Arago, 75014 Paris, France

[27]Astrophysics Research Institute, Liverpool John Moores University, Twelve Quays House, Egerton Wharf, Birkenhead CH41 1LD, UK

[28]SUPA, University of St Andrews, School of Physics & Astronomy,North Haugh, St Andrews, KY16 9SS, UK

[‡]Royal Society University Research Fellow

[29]University of Tasmania, School of Mathematics and Physics, Private Bag 37, Hobart, TAS 7001, Australia

[30]Observatoire Midi-Pyrénés, Laboratoire d'Astrophysique, UMR 5572, Université Paul Sabatier–Toulouse 3, 14 avenue Edouard Belin, 31400 Toulouse, France

[31]Department of Physics and Astronomy, Dartmouth College, 6127 Wilder Laboratory, Hanover, NH 03755, USA

[32]University of Oxford, Denys Wilkinson Building, Keble Road, Oxford, OX1 3RH, UK

**Searches for extrasolar planets have uncovered an astonishing diversity of planetary systems, yet the frequency of solar system analogs remains unknown. The gravitational microlensing planet search method is potentially sensitive to multiple-planet systems containing analogs of all the solar system planets except Mercury. We report the first detection of a multiple-planet system with microlensing. We identify two planets with masses of ∼ 0.71 and ∼ 0.27 times the mass of Jupiter and orbital separations of ∼ 2.3 and ∼ 4.6 astronomical units orbiting a primary of mass ∼ 0.50 solar masses. This system resembles a scaled version of our solar system in that the mass ratio, separation ratio, and equilibrium temperatures of the planets are similar to those of Jupiter and Saturn. These planets could not have been detected with other techniques; their discovery from only 6 confirmed microlensing planet detections suggests that solar system analogs may be common.**

Nearly 250 extrasolar planets (*1*) have been discovered by measuring a variety of effects: reflex motion of the host star using pulsar timing or precision Doppler measurements (*2–4*); periodic dimming of the parent star as the planet transits in front (*5, 6*); and planet-induced perturbations to microlensing light curves in which the host star acts as the primary gravitational lens (*7–10*). These detections have uncovered an enormous range of planetary properties, indicating that planetary systems very unlike our own are common throughout the Galaxy. In particular, ∼ 5% of main-sequence stars with masses of $0.3 − 2\ M_\odot$ host giant planets with periods less than four years (*11*).

To date, ∼ 25 multiple-planet systems have been detected (*12*), all but one (*2*) using the Doppler method. Since Doppler surveys must monitor the host star's reflex motion over the planet's orbital period, they are limited by the finite duration as well as the sensitivity of the measurements. Hence, they are only just now becoming sensitive to Jupiter analogs and are not yet sensitive to Saturn analogs (nor, ipso facto, Jupiter/Saturn systems). Thus, all multiple-planet systems discovered so far are very dissimilar from our own, and the frequency of solar system analogs remains unknown.

Since microlensing relies on the direct perturbation of light from distant stars by the gravitational field of the planet, rather than on indirect dynamical effects of the planet on the host star, it is 'instantaneously' able to detect planets without requiring observations over a full orbit. For a primary of mass $M$, microlensing sensitivity peaks for planets in the range ∼ $[1 − 5](M/0.3M_\odot)^{1/2}$ astronomical units (AU) (*13*). For solar-mass stars, this is exactly the range of the solar system gas giants so microlensing provides a method to probe solar system analogs (*14*).

Planets reveal themselves in microlensing events via two different channels. In the main channel, the planet perturbs one of the two images created by the primary lens (i.e., the host star) (*13*). Since the planet/star mass ratio $q = m/M$ is small, the portion of the magnification pattern that it perturbs is likewise small. Hence, the deviation is short [$t_p \sim 1\,(m/m_j)^{1/2}$ day where $m_j$ is the mass of Jupiter] compared to the primary event timescale ($t_{\rm E} \sim 1$ month). Furthermore, because the planet location is random relative to the source trajectory, the probability of detecting a planet (even if it is present) is only $\sim 10\%(m/m_j)^{1/2}$. Thus detecting planets via this channel requires continuous, dense sampling of many events (*14*). If the frequencies of individual planets in multiple-planet systems are independent, then the probability of detecting two planets in this channel is just the square of detecting one and is therefore very small.

A decade ago, Griest & Safizadeh (*15*) pointed out a secondary channel that is extremely sensitive to planets, but is accessible only for the very rare class of high-magnification ($> 100$) events. Near the peak of high-magnification events, the two images created by the primary star are highly magnified and distorted and form a complete or nearly complete Einstein ring. A planetary companion to the primary star lying reasonably near the Einstein ring, in addition to perturbing its own small local neighborhood, will also distort the symmetry of the ring. As the host passes very close to the source line-of-sight, the images sweep around the Einstein ring, thus probing this distortion. While the total number of planetary perturbations in this channel is substantially smaller than in the main channel, the instantaneous chance of detection is much higher and, equally important, the interval of high sensitivity (i.e., high-magnification) is predictable from the evolution of the light curve (*15–18*). This permits concentration of scarce observing resources on these events. Furthermore, the high-magnification makes it possible to acquire high signal-to-noise ratio photometry of the peak of the events using relatively small-aperture (and so plentiful) telescopes. As a result, 4 (*8, 10*) of the 6 planets (*7, 9*) discovered to date in microlensing events were in high-magnification events.

Almost immediately, Gaudi et al. (*19*) derived an important corollary: since planets in the neighborhood of the Einstein ring are revealed with near unit probability in high-mag events, multiple-planet systems lying in this region will be revealed with almost the same probability (*19*).

Currently, planets are detected in microlensing events toward the Galactic bulge via an alert/follow-up system. Because the microlensing event rate toward the bulge is $\mathcal{O}(10^{-6})$ per star per year, the Optical Gravitational Lens Experiment (OGLE) (*20*) and Microlensing Observations for Astrophysics (MOA) (*18*) collaborations each monitor about $10^8$ stars over about 20 deg$^2$ in the Galactic bulge and together alert $\sim 700$ ongoing microlensing events per year. Two collaborations, a joint venture of the Probing Lensing Anomalies NETwork (PLANET) (*21*) and RoboNet (*23*) collaborations, and the Microlensing Follow Up Network ($\mu$FUN) (*22*), then monitor a subset of these alerts to search for planets.

$\mu$FUN focuses almost entirely on high-mag events, including two events originally alerted by OGLE that proved to have a Jupiter-mass (*8*) and a Neptune-mass (*10*) planet, respectively. Here we report on the first detection of a multi-planet system using this approach.

On 26 March 2006 (HJD$\sim 3820$), the OGLE Early Warning System (EWS) (*20*) announced

4

OGLE-2006-BLG-109 as a probable microlensing event and on 28 March broadcast a "low amplitude anomaly" (0.1 mag) alert, remarking that it could "be a signature of a planetary companion". This immediately triggered followup observations by $\mu$FUN and RoboNet, which gained intensity as it became clear that the event was approaching very-high magnification. On 5 April, it reached a peak magnification $A = 550$, the third highest recorded for any microlensing event at that time, and underwent a deviation from the single-lens form indicative of a binary lens. Within 12 hours of this deviation, a preliminary model indicated a Jovian-class planet, which was predicted to generate an additional peak on 8 April. Observations were further intensified. The 8 April peak occurred as predicted, but in the meantime, there was an additional peak on 5-6 April, which turned out to be due to a second Jovian-class planet.

The resulting light curve (Fig. 1) shows data from 11 observatories, including 7 from $\mu$FUN [the Auckland 0.35m and Farm Cove 0.25m in New Zealand (clear filter), the Wise 1m in Israel (clear), the CTIO/SMARTS 1.3m in Chile ($I$-band and $H$-band), the AREO8 0.3m in New Mexico operated by the Campo Catino Astronomical Observatory (clear), and the MDM 2.4m ($I$-band) and Mt. Lemmon 1.0m ($I$-band) in Arizona], the OGLE Warsaw 1.3m ($I$-band) in Chile, the MOA Mt. John 0.6m ($I$-band) in New Zealand, the PLANET/Canopus 1m ($I$-band) in Tasmania, and the RoboNet/Liverpool 2m ($R$-band) in the Canary Islands. There are a total of 2642 data points. In addition, there are 29 V-band data points from OGLE and CTIO/SMARTS that we use to determine the source color, which is crucial for measuring the size of the planetary system (*22*). Details of the data reduction will be presented elsewhere (*24*).

The qualitative character of the event can be read directly off the light curve, primarily from the 5 distinctive features shown in Figure 2. Consider the first 3 features: the low-amplitude anomaly (OGLE, HJD$\sim 3823$) that triggered the OGLE EWS alert, the gentle "shoulder" during the first rise (MOA, HJD$\sim 3830$), and the first peak (Auckland, HJD$\sim 3831$). Together, these can only be produced by, respectively, passage close to or over a weak cusp, entrance into a weak caustic, and exit from a strong caustic. [The magnification diverges on closed concave caustics due to the appearance (when entering) or disappearance (when exiting) of additional images within the enclosed area. Caustics are strong or weak depending on the brightness of these images. The concave curves meet at cusps which are higher-order singularities in the lens mapping and produce sharp spikes of magnification when crossed by the source.] Such a sequence requires a topology similar to the one shown in the inset to Figure 1. The specific strengths of the three features requires the specific geometry shown in the figure. In particular, the narrow mouth of the caustic toward the bottom generates a very strong caustic. This was essentially the argument used to predict the fifth feature (MDM/Lemmon/Auckland/FarmCove/Tasmania, HJD$\sim 3834$), corresponding to a moderately strong cusp passage (Fig. 1). The size and strength of this caustic imply a Jovian-class planet lying very close to the Einstein ring, although detailed modeling is required to derive the precise planet/star mass ratio. The fourth feature (Wise/OGLE, HJD$\sim 3831.5$) cannot be explained by considering the caustic generated by this Jovian-class planet alone. This feature occurs near the time when the source approaches the closest to the center-of-mass of the planet/star system; this is exactly the time at which the central-caustic bumps due to additional planets are expected to occur (*19*). The inset in Fig-

5

ure 1 highlights the additional caustic feature due to a second planet that is required to explain this bump. This caustic feature must be smaller than the main caustic, which implies that the planet, also of Jovian class, lies farther from the Einstein ring, although a detailed analysis (*15, 24*) is required to show that it lies inside rather than outside the Einstein ring and is almost 3 times heavier than the first planet. We label these planets "OGLE-2006-BLG-109Lc" and "OGLE-2006-BLG-109Lb", respectively. Although the caustics of the individual planets do interact to form a single caustic curve, their effects are nevertheless mostly independent (*17, 25*) and so the parts of the caustic associated with the individual planets can be identified, as shown in Figure 1. Modeling the light curve in detail with a three-body lens yields, $m_b/M = 1.35 \times 10^{-3}$, $m_c/m_b = 0.36$ for the mass ratio of the planets and their host, very similar to $m_j/M_\odot = 0.96 \times 10^{-3}$ and $m_s/m_j = 0.30$ for Jupiter, Saturn, and the Sun. The ratio of projected separations $r_{\perp,b}/r_{\perp,c} = 0.60$ is also very similar to the Jupiter/Saturn value of $a_j/a_s = 0.55$.

There are several higher-order effects apparent in this event that will permit us to extract much more detailed information about the system from the light curve. We only briefly sketch these here. For over 95% of microlensing events, the lens parameters are determined only relative to the angular Einstein radius $\theta_E$, whose absolute scale remains unknown. Here $\theta_E = \sqrt{\kappa M \pi_{rel}}$, where $M$ is the mass of the lens, $\pi_{rel}$ is the relative lens-source parallax, and $\kappa \equiv 4G/c^2\mathrm{AU}$ is a constant. However, in this event the effect of the finite size of the source star during caustic exit allows us to measure the source radius relative to the Einstein radius, $\rho = \theta_*/\theta_E$ (*26*). From the source color, we infer its surface brightness, and so from its flux we can determine its angular size $\theta_*$, and thus $\theta_E$ (*22*).

The acceleration of Earth in its orbit about the Sun induces subtle distortions on the light curve called microlens parallax, which yields another measure of the Einstein radius, $\tilde{r}_E \equiv \mathrm{AU}/\pi_{rel}$, its physical size projected onto the observer plane (*27*). This is usually measured only in the roughly 3% of events that are extremely long, but this event happens to be long, with $t_E = 129$ days, and so displays clear distortions arising from parallax.

Combining these two measures of the Einstein radius allows us to triangulate the event and so determine the host star distance, $D_l = 1/(\theta_E/\tilde{r}_E + 1/D_s)$, and mass, $M = (c^2/4G)\tilde{r}_E\theta_E$, where $D_s = 8$ kpc is the distance to the source. Based on a preliminary analysis we infer $D_l \simeq 1.5$ kpc and $M \simeq 0.5\,M_\odot$. Based on high-resolution Keck AO $H$-band images, we detect light from the lens and infer its magnitude to be $H = 17.17 \pm 0.25$, consistent with the mass estimate from the light curve. We subsequently incorporate the lens flux constraint in the light curve analysis, which allows us to derive more precise estimates of the lens mass and distance of $D_l = (1.49 \pm 0.13)$ kpc and $M = (0.50 \pm 0.05)\,M_\odot$. The planet masses are $m_b = 0.71 \pm 0.08$ and $m_c = 0.27 \pm 0.03$ times the mass of Jupiter.

Finally, we also detect the orbital motion of the outer planet; this motion both rotates and changes the shape of the larger caustic shown in the top inset to Figure 1. Most dramatically, without allowing for the planet's revolution about the star, the source trajectory cannot be made to both graze the first cusp and exit the caustic at the peak in the way that it does. We are able to constrain the two components of the projected velocity of the planet relative to the primary star.

These two components imply a projected velocity of the planet of $9.8$ km/s. These two components, together with stellar mass estimated from the finite source effect and microlens parallax, completely determines the outer planet's orbit (including inclination) under the assumption that it is circular, up to a two-fold degeneracy. These two degenerate solutions are marginally distinguished by the data via the effect of the planet's acceleration on the light curve. Thus we can estimate the full (three-dimensional) separation of planet c (again assuming a circular orbit), and also of planet b (assuming a coplanar and circular orbit). We find $a_b = (2.3 \pm 0.2)$ AU and $a_c = (4.6 \pm 0.5)$ AU. A more refined estimate of these parameters and their uncertainties requires a detailed analysis including the combined effects of finite sources, parallax, and orbital motion of the planets. The results of this analysis will be presented elsewhere (*24*).

The OGLE-2006-BLG-109L planetary system bears a remarkable similarity to own solar system. Although the primary has a mass of only 50% that of the Sun, the mass ratio of the two planets ($0.37$) and separation ratio ($0.60$) are similar to those of Jupiter and Saturn. We infer their equilibrium temperatures to be $T_{\mathrm{eq}} \sim (82 \pm 12)$ K and $T_{\mathrm{eq}} \sim (59 \pm 7)$ K, $\sim 30\%$ smaller than those of Jupiter and Saturn.

Prior to the detection of extrasolar planets, planet formation theories generally predicted that other systems should resemble our solar system. In the core-accretion paradigm, the most massive giant planet forms at the 'snow line,' the point in the protoplanetary exterior to which ices are stable. Immediately beyond the snow line, the surface density of solids is highest and the dynamical time is the shortest, and therefore the timescale for planet formation is the shortest. Exterior to the snow line the formation timescale decreases with distance from the host star as the surface density decreases and the dynamical time increases. Thus in this 'classical' picture of planet formation, one would expect planet mass to decrease with increasing distance beyond the snow line, as is observed in our solar system (*28*). The discovery of a population of massive planets well interior to the snow line demonstrated that this picture of planet formation is incomplete, and significant inward migration of planets must occur during or subsequent to their formation (*29*). Nevertheless, it is likely that this classical picture is still applicable to our solar system and may be applicable to some fraction of other systems as well. The OGLE-2006-BLG-109L planetary system represents just such a 'scaled version' of our own solar system, with a less-massive host. This system preserves the mass-distance correlation in our solar system, and the scaling with primary mass is consistent with the core-accretion paradigm in which giant planets that form around lower-mass stars are expected to be less massive but form in regions of the protoplanetary disk with similar equilibrium temperatures and are therefore closer in to their parent star for lower mass hosts (*30*).

The majority of the $\sim 25$ known multi-planet systems are quite dissimilar to the OGLE-2006-BLG-109L system and to our own solar system. Many of these systems have very close-in massive planets with separations well inside the snow line which are indicative of large-scale planetary migration, or have a 'normal hierarchy' in which the mass of the giant planets increases with distance from the parent star. There are two multi-planet systems with properties roughly similar to those of OGLE-2006-BLG-109L. The 47 UMa and 14 Her systems each contain a giant planet at a semimajor axis of $\sim 3$ AU, along with a second, less massive giant

planet at a separation of $\sim 7$ AU (*31*). However the host stars in these systems are considerably more massive than OGLE-2006-BLG109L. Thus the equilibrium temperatures of the planets in 47 UMa and 14 Her systems are considerably higher than those of OGLE-2006-BLG109L or Jupiter and Saturn, and so these systems cannot be considered close analogs of our solar system.

OGLE-2006-BLG109Lb,c are the fifth and sixth planets to be detected via microlensing. Although, given the detection of planet c, the *a priori* probability of detecting planet b in this event was high, it was not unity. Furthermore, only two other Jovian-mass planets have been detected via microlensing (*7,8*), and neither event had substantial sensitivity to multiple planets. These facts may indicate that the stars being probed by microlensing that host Jovian-mass companions are also likely to host additional planets. If the OGLE-2006-BLG-109L planetary system is typical, these systems may have properties similar to our solar system. Regardless, the detection of the OGLE-2006-BLG-109L planetary system demonstrates that microlensing surveys will be able to constrain the frequency of solar system analogs throughout the Galaxy.

# References and Notes

1. J. Schneider (2006); http://vo.obspm.fr/exoplanetes/encyclo/encycl.html

2. A. Wolszczan, D. A. Frail, *Nature* **355**, 145 (1992).

3. M. Mayor, M., D. Queloz, D. *Nature* **378**, 355 (1995).

4. G. W. Marcy, & R. P. Butler, *Astrophys. J.* **464**, L147 (1996).

5. A. Udalski, et al. *Acta Astron.* **52**, 1 (2002).

6. M. Konacki, et al. *Nature* **421**, 507 (2003).

7. I. A. Bond, et al., *Astrophys. J.* **606**, L155 (2004).

8. A. Udalski, et al. *Astrophys. J.* **628**, L109 (2005).

9. J.-P. Beaulieu et al., *Nature* **439**, 437 (2006).

10. A. Gould, et al. *Astrophys. J.* **644**, L37 (2006).

11. D. A. Fischer, J. Valenti, *Astrophys. J.* **622**, 1102 (2005).

12. R. P. Butler, et al., *Astrophys. J.* **646**, 505 (2006).

13. A. Gould, A. Loeb, *Astrophys. J.* **396**, 104 (1992).

14. D. B. Bennett, S. H. Rhie, *Astrophys. J.* **574**, 985 (2002).

15. K. Griest, N. Safizadeh, *Astrophys. J.* **500**, 37 (1998).

16. S. H. Rhie, et al., *Astrophys. J.* **533**, 378 (2000).

17. N. J. Rattenbury, I. A. Bond, J. Skuljan, P. C. M. Yock, *Mon. Not. R. Astron. Soc.* **335**, 159 (2002).

18. F. Abe, F., et al., *Science* **305**, 1264 (2004)

19. B. S. Gaudi, R. M. Naber, P. D. Sackett, *Astrophys. J.* **502**, L33 (1998).

20. A. Udalski, *Acta Astron.* **53**, 291 (2003).

21. M. Albrow, *Astrophys. J.* **509**, 687 (1998).

22. J. Yoo, et al., *Astrophys. J.* **603**, 139 (2004).

23. M.J. Burgdorf, et al., *Planetary and Space Science* **55**, 582 (2007)

24. D. B. Bennett, et al. in preparation (2008).

25. C. Han, 2005, *Astrophys. J.* **62**9, 1102

26. A. Gould, *Astrophys. J.* **421**, L71 (1994).

27. A. Gould, *Astrophys. J.* **392**, 442 (1992).

28. J. J. Lissauer, *Icarus* 69, 249 (1987).

29. D. N. C. Lin, P. Bodenheimer, D. C. Richardson, *Nature* **380**, 606 (1996)

30. S. Ida, & D. N. C. Lin, *Astrophys. J.* **626**, 1045 (2005)

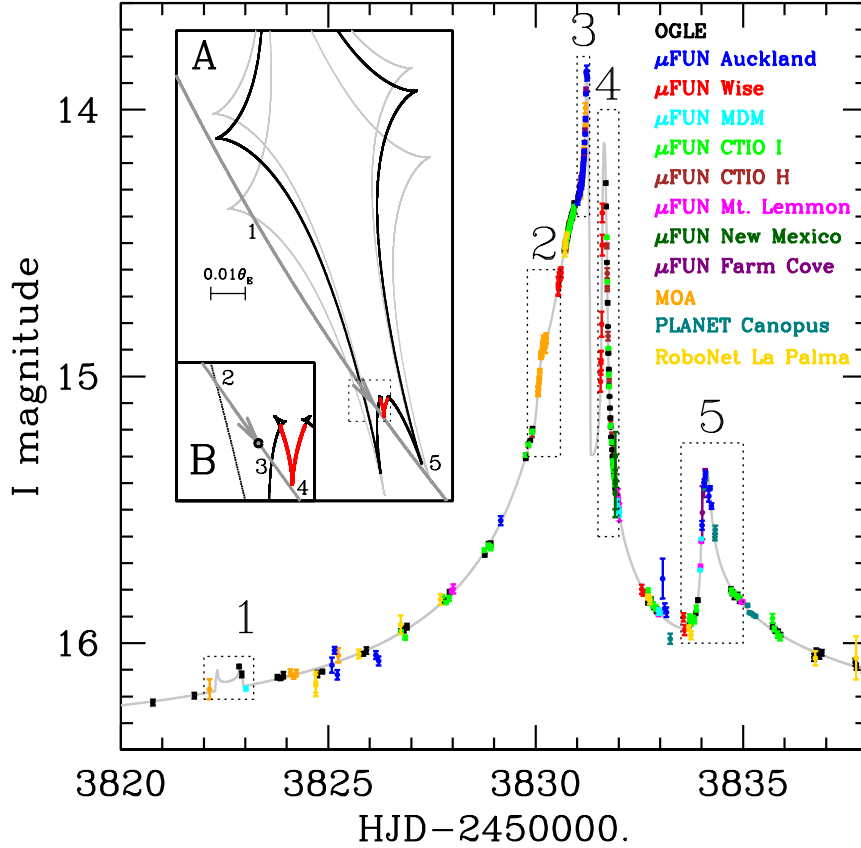31. R. A. Wittenmyer, R. A., *Astrophys. J.* **654**, 625 (2007)

Figure 1: Data and best-fit model of the OGLE-2006-BLG-109Lb,c two-planet system. The data have been binned for clarity, although the fitting procedures used the unbinned data. Only data near the peak of the event are shown (the unlensed magnitude of the event is $I = 16.42$). Panel A: The source trajectory through the caustic created by the two-planet system is shown as the dark grey curve with the arrow indicating the direction of motion. The horizontal line shows an angular scale of $0.01\ \theta_{\rm E}$, or $\sim 15\ \mu$as. The shape and orientation of the caustic due to both planets at the peak of the event is shown by the black curve. The 5 light curve features detailed in Fig. 2 are caused by the source crossing or approaching the caustic; the approximate locations of the features are labeled with numbers. The majority of the caustic (in black) is due to only the outer (Saturn-analog) planet; this portion of the caustic explains 4 of the 5 features. The portion of the caustic arising from the second (Jupiter-analog) planet is highlighted in red. This additional cusp in the caustic is required to explain the fourth feature in the light curve; as such the fourth feature signals the presence of a second (Jupiter-analog) planet. Due to the orbital motion of the Saturn-analog planet, the shape and orientation of the caustic changes over the course of the event. The light grey curves show the caustic at the time of features 1 and 5. Panel B: A zoom of the source trajectory and caustic near the times of the second, third, and fourth features. The circle shows the size of the source.
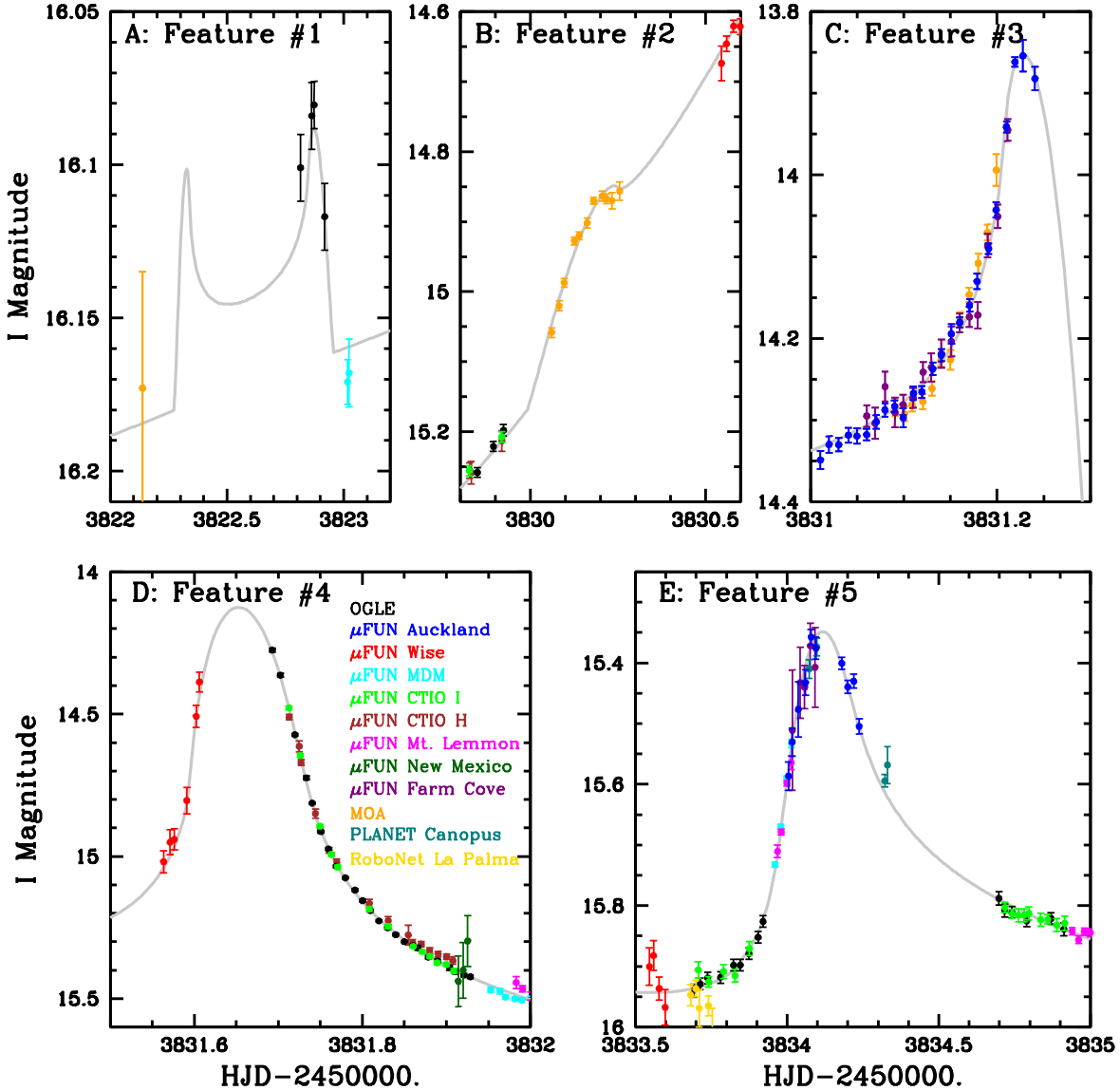
10

Figure 2: Five features of light curve from Fig. 1, which determine planetary geometry. A) Feature #1: weak cusp approach; B) Feature #2: weak caustic entrance; C) Feature #3: strong caustic exit; D) Feature #4: strong cusp approach; E) Feature #5: moderate cusp approach. Features 1, 2, 3, and 5, are explained by the black portion of the caustic seen in Panel A of Fig. 1. Feature 4 requires an additional cusp in the caustic, which is shown as the red curve. Data have been binned for clarity.